Received: Added at production | Revised: Added at production | Accepted: Added at production

DOI: xxx/xxxx

ORIGINAL RESEARCH PAPER

A semi-analytical Gaussian beam summation method to compute the RCS of dielectric and dielectric-coated targets in mono or bi-static configurations

Thomas Bonnafont[1] | **Mira Kaissar Abboud**[1] | **Ali Khenchaf**[1] | **Philippe Pouliguen**[2]

[1]Lab-STICC, UMR CNRS 6285, Institut Polytechnique de Paris, 29806 Brest, France

[2]DGA-AID, 60 Bd. du général Martial Valin, Paris 75509, France

Correspondence
Corresponding author Thomas Bonnafont.
Email: thomas.bonnafont.enac@gmail.com

Funding Information
This research was supported by the The authors would like to thank the AID-DGA (Defense Innovation Agency - Directorate General of Armaments) for their support of this research work carried out within the framework of the HyMEF project

Abstract

This study proposes to extend and refine the methodology of Gaussian beam summation (GBS) for computing the radar cross section (RCS) of dielectric targets in both monostatic and bistatic cases. Furthermore, the generalization to the bi-static case is shown to be equivalent to phase steering. Indeed, we leverage a semi-analytical GBS technique, inspired by optical physics. We compute the RCS by discretizing the target, such as with rectangles or triangles, and then summing the contributions of these discrete elements, for which the expansion coefficients (or weight function) have already been computed. This allows, first, to relax the far-field criteria to the scale of the discretized elements and, second, to facilitate the computation of the RCS of more complicated targets. Furthermore, dielectrics are accounted for using the Fresnel coefficient. Numerical tests and applications in the S and X bands are also provided to validate the method by comparing it to analytic RCS formula, and highlight its advantages. We also propose to study the case where the dielectric parameters of the target are not perfectly known.

KEYWORDS
electromagnetic, RCS, asymptotic methods, Gaussian beam, Gaussian beam summation

1 | INTRODUCTION

Computing the radar cross section (RCS) of targets is of major importance for numerous applications in detection, e.g., target[1,2] or oil leakage[3,4,5] detection, and imaging, e.g,. synthetic aperture radar (SAR)[6] or inverse scattering[7]. Indeed, assuming we are in free space and the target position is known, it is the last unknown of the radar equation

$$P_r = P_t G_t G_r \left(\frac{\lambda}{4\pi R_t R_r}\right)^2 \sigma, \tag{1}$$

where the under-script r and t stand for receiver and transmitter, P for the power, G the gain, R the distance with the target, λ the wavelength and σ to the RCS. In particular, it is the quantity we need to minimize to avoid detection, for example, of wind turbines so that they do not perturb the radar signal[8,9,10], or of planes and drones in warfare scenarios[11,12]. Therefore, lots of new shapes and materials have been proposed in this sense in recent years[10,13,12,14], enforcing the need for fast and reliable methods to compute the RCS[15]. Furthermore, rapid RCS predictions can help detection algorithm or the optimization of radar systems. Thus, fast and reliable methods to compute the RCS of a given target are still an ongoing topic in the electromagnetic community.

To this end, one can think of rigorous methods such as the method of moments (MoM)[16,17,18], the finite difference time domain (FDTD)[19,20,21,22,23] or the finite elements (FEM)[24,25,26]. Still, they are limited when the size of the object becomes electrically large due to their mesh requirement, i.e., of order $\lambda/10$. Thus, some hybrid methods have been proposed, such as FEM and MoM[27,28] to overcome some of the issues, but the computation time remains large for this context.

This is why asymptotic methods are commonly used to compute the RCS of large objects, for example, geometrical optic[29,30,31,32] or physical optic (PO)[30,33,32] methods. Both assume that the field is a sum of plane waves and are valid in the high-frequency regime. In particular, the PO is widely utilized[34,35,2,36,37] in our context. Indeed, as the high-frequency counterpart of the MoM, it is based on meshing only the surface of the target, leading to fewer unknowns. The main idea of the PO is to compute the field at the observation point using the far field approximation of the Stratton-Chu formula, assuming the incident field is a plane wave and the currents are constant over each facet.

Abbreviations: ANA, anti-nuclear antibodies; APC, antigen-presenting cells; IRF, interferon regulatory factor.

Nonetheless, at first order PO does not consider diffraction by edges, but this can be overcome using higher order approximations such as the physical theory of diffraction [38,39,40] or the modified equivalent current theory [41,42,43]. Finally, even if they are particularly efficient and can accommodate complicated structures the main drawback of this method is the singular points [44] associated with the Green kernel, which can lead to caustics in geometrical optics, of problems near shadow boundaries for the PO. Nonetheless, some of this limitations can also be overcome by improving the quadrature used in PO for example.

To overcome this problem, Gaussian beams (GB) have been suggested in the 80s [45,46,47]. Indeed, as a solution of the parabolic wave equation, they can be used in place of plane waves and do not exhibit any singular points [48]. Later on, numerous methods have been developed in the electromagnetic community to use this approach either to compute the RCS [49,50,51,52], the propagation of the field in quasi-optic regime [53], to study large aperture array antennas [54] or lens antennas [55,56]. In the particular context of RCS, two methods are commonly used, either the Gaussian beam launching (GBL) or the Gaussian beam summation (GBS) [49,57,50]. The first can be seen as the GB counterpart of the ray launching, the incident field is decomposed as a sum of GB, while the second is the one of the PO. Indeed, we consider an incident plane wave on the target that induces a current considered constant over each facets that excite a GB toward the observation. This strategy has recently been generalized to the case of a dielectric cuboid [52], where the PO calculated RCS is matched using a steepest descent. It shall be noted that avoiding the singular points come at the cost of some computational resources and the need to match the gaussian beam expansion.

Nonetheless, when considering a complex target, it is not always possible to directly match the PO computed RCS. Thus, in this article, we propose first to develop a semi-analytic GBS approach that uses either a triangle or a quadrangular mesh of the target. Furthermore, using Fresnel coefficients, we consider either dielectric or dielectric-coated targets. Finally, the semi-analytic approach allows us to consider the bistatic case as a direct extension using phase steering, which constitutes an important improvement since, to the author's knowledge, only the mono-static case has been studied before. Nonetheless, since this is a first step toward a GBS for dielectric-coated target in particular in the bistatic case, this method has still some limits. For example, even if the UTD or GTD can be integrated, as we will see with an example in the numerical tests, the proposed method is still limited to simple structures. If the diffraction is not considered, the method can be easily generalized to more complicated objects since all the proposed approach is based on the underlying mesh contrary to [52].

The remainder of this article is organized as follows. Section 2 introduced the problem setting and the proposed semi-analytic Gaussian beam summation method. In Section 3, numerical tests are performed in the S and X bands to validate the method against an analytic solution in a PO setting and highlight the advantages of the proposed approach. Furthermore, a PCE-based approach is proposed to account for uncertainty over the dielectric parameters of the considered material. Finally, Section 4 concludes the paper and gives a perspective for future works.

2 | METHOD

2.1 | Problem setting and notations

Throughout this article, we assume an $\exp(-j\omega t)$ time variation of the field, with $\omega = 2\pi f_0$ the angular frequency and f_0 the associated frequency such that we are in the high frequency regime. Also, the vectors are denoted in bold font, such as $\mathbf{U}$, and lower case bold font when normalized, such as $\mathbf{u} = \mathbf{U}/\|\mathbf{U}\|_2$. The usual notation $\mathbf{E}$ and $\mathbf{H}$ are used for the electric or magnetic fields, respectively. Furthermore, we assume to compute the field in the far-field of the target such that $r \geq 2D^2/\lambda$ with D the largest dimension of the target and λ the wavelength.

We are interested in computing the RCS, denoted by σ, of a dielectric, or dielectric-coated target, at the boundary of a given domain Ω, which consists of free space. We thus need to compute

$$\sigma = \lim_{r\to\infty} 4\pi r^2 \frac{\|\mathbf{E}^s\|_2^2}{\|\mathbf{E}^i\|_2^2}, \tag{2}$$

where the upper scripts s and i are for the scattered and incident fields. Since $\mathbf{E}^i$ is assumed to be a plane wave of incident angle θ_i known, our goal is to compute $\mathbf{E}^s$. The normalized RCS in dBm^2 is calculated as $\sigma/(S\lambda^2)$, with S the object surface. A schematic representation of the situation is given in Figure 1. Note that in the case of dielectric coating, the inside medium corresponds to a perfect electric conductor (PEC), and that all can be generalized to more than 2 media. Finally, in this work we assume $\varepsilon_j \in \mathbb{C}$, with

$$\varepsilon_j = \varepsilon_0\varepsilon_{rj} - j\frac{\sigma_j}{\omega}, \tag{3}$$

where ε_{rj} is the relative permittivity of the medium j and σ_j its conductivity.

Finally, we assume the target boundary to be Lipschitz continuous but to not restrict our self to star domain for the theoretical development. We also assume the coating to have uniform dielectric properties, but it can be constituted of different layers.

2.2 | Gaussian beams as asymptotic solutions

In this section, we do a brief reminder on the Gaussian beams that are solutions of the parabolic wave equation, and thus asymptotic solutions of the Helmholtz equation.

Let us consider the Γ_0-ray centered coordinates system (s, q_1, q_2), pictured in Figure 2. This corresponds to the system of coordinates used

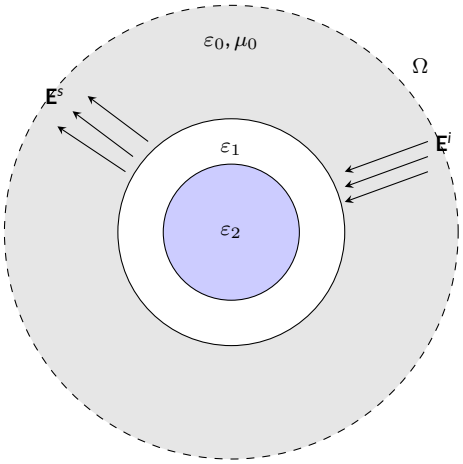

FIGURE 1 A schematic representation of the problem. The goal is to compute the RCS of the target in Ω.

in ray tracing or to solve the equation using the method of characteristics. Here, s corresponds to the length along the ray Γ_0 and (q_1, q_2) to the normal distance to this ray.

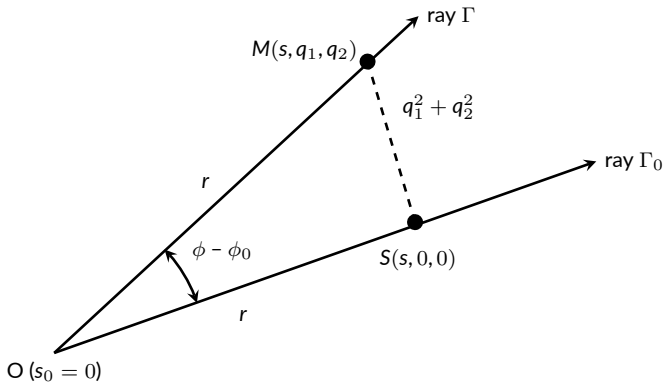

FIGURE 2 New ray centered coordinates system (s, q_1, q_2) around the ray Γ_0.

In this coordinates system omitting the $\exp(j\omega t)$ time variation, and setting

$$u(s, q_1, q_2) = \sqrt{c_0} \exp\left(j\omega \int_0^s \frac{ds}{c_0}\right) W(s, q_1, q_2), \tag{4}$$

with c_0 the wave velocity in free space. The latter corresponds to the reduced field[‡] and is different to[45] since Ω corresponds to free-space here. Furthermore, the assumption that n is slowly varying in the computational domain is directly fulfilled here. Indeed, for the RCS, we are only interested in the field $\mathbf{E}^s$ computed far from the target in Ω, and not inside it. Also, in (4), the function W is solution of

$$\frac{2j}{c_0}\frac{\partial W}{\partial s} + \frac{\partial^2 W}{\partial q_1^2} + \frac{\partial^2 W}{\partial q_2^2} = 0, \tag{5}$$

corresponding to the parabolic wave equation (PWE) in free space. It shall be noted that the PWE is a paraxial approximation of the Helmholtz equation, thus the Gaussian beam are only solutions in a paraxial cone of $\phi_{\max}$ around the propagation direction.

In[45,46], they have shown that we can look for the solution of (5) as a Gaussian beam, with

$$W(s, q_1, q_2) = \sqrt{\frac{c_0}{\det(Q(s))}} \exp\left(j\omega\frac{s}{c_0} + j\frac{\omega}{2} q^T P(s) Q(s)^{-1} q\right), \tag{6}$$

where P and Q are solutions of the following ordinary differential equations (ODE)

$$\begin{aligned} \tfrac{dP(s)}{ds} &= 0, & P(0) &= \tfrac{1}{c_0} I, \\ \tfrac{dQ(s)}{ds} &= c_0 P(s), & Q(0) &= \tfrac{-j\omega\omega_0^2}{2c_0} I, \end{aligned}$$

where ω_0 corresponds to the half beam width, for which an optimal value can be computed for a given distance s[45,46]

$$\omega_0 = \sqrt{\frac{2c_0}{\omega} s}. \tag{7}$$

The initial conditions correspond to the Hill's one[58], and ensure that the Gaussian beam exists with $Q \neq 0$ and $\mathrm{Im}(PQ^{-1}) > 0$ even if $s = 0$. Thus, it shall be noted that there are no singularities for the Gaussian beam, contrary to when using ray-based methods, i.e., singularities of the Green kernel. Then, by solving this system of ODEs, we can compute the solution W, i.e., a Gaussian beam from a source point to a receiver placed at $M = (s, q_1, q_2)$.

2.3 | The semi-analytic Gaussian beam summation method

First, let us assume that the target is a PEC for readability and assume locally plane interfaces, thus placing ourselves within the PO framework. The case of dielectric targets will be treated as a direct extension afterward. In this case, the electric and magnetic currents are given by

$$\begin{aligned} \mathbf{J} &= 2\mathbf{n} \times \mathbf{H}^i, \\ \mathbf{M} &= 0, \end{aligned} \tag{8}$$

where $\mathbf{H}^i$ is the incident magnetic plane wave related to $\mathbf{E}^i$ by

$$\mathbf{H}^i = \frac{1}{Z}\mathbf{k}_i \times \mathbf{E}^i, \tag{9}$$

with Z the media impedance. For example, assuming a vertical polarization (V-polar), we have $\mathbf{E}^i = E_0 \exp(jk\mathbf{k}_i \cdot \mathbf{r})\mathbf{e}_\theta$ in the usual $(\mathbf{r}, \mathbf{e}_\theta, \mathbf{e}_\phi)$ spherical coordinate system. Then, from this current, we can derive the scattering field as

$$\mathbf{E}^s = jk\mathbf{k}_s \times \int_S \left(\mathbf{k}_s \times \mathbf{J}(\mathbf{R}')\right) \frac{\exp(jk\|\mathbf{k}_s - \mathbf{R}'\|_2)}{4\pi\|\mathbf{k}_s - \mathbf{R}'\|_2} dS', \tag{10}$$

[‡] Indeed, a factorization by the variation in the propagation direction has been done.

where S corresponds to the surface of the target and $\mathbf{k}_s$ to the scattering wave vector. In the same way as for semi-analytic or numeric PO, we approximate the surface integral with a quadrature as

$$\mathbf{E}^s = jk\mathbf{k}_s \times \sum_{\tau \in S_h} \left(\mathbf{k}_s \times \mathbf{J}(\mathbf{R}'_\tau)\right) \frac{\exp(jk\|\mathbf{k}_s - \mathbf{R}'_\tau\|_2)}{4\pi\|\mathbf{k}_s - \mathbf{R}'_\tau\|_2}|\tau|, \tag{11}$$

where S_h is a partition of the surface S of the considered object, and $|\tau|$ the measure of one cell $\tau \in S_h$. One one the main problems in this expression is the approximation of the Green kernel. Indeed, the latter exhibits some singularities[44].

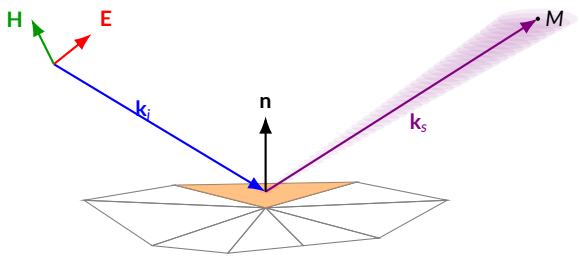

FIGURE 3 Schematic representation of the semi-analytic Gaussian beam summation method with a triangular mesh.

The idea of the semi-analytical GBS method is thus to replace the Green kernel in expression (11) by a Gaussian beam fan, see Figure 3 for a schematic representation. Indeed, the incoming wave is still assumed to be a plane wave, while the outgoing one is now a Gaussian beam. Therefore, the scattered field at the receiving point M can be expressed as

$$u(M) = \int_\gamma F(\phi) u_\phi(s, q_1, q_2) d\gamma, \tag{12}$$

where ϕ is the take-off angle of a given Gaussian beam, and γ to the integration surface, i.e., the area of effective take-off angles, and $d\gamma = \sin(\phi) d\phi d\theta$ where $\theta \in [0, 2\pi[$. Since the Gaussian beams are solutions of the PWE (5), we have $\phi_{\max} \leq 45°$, corresponding to the valid paraxial cone. The idea is to sum all the Gaussian beams that effectively contribute to the field at the receiver point M with a given weight F. Indeed, the latter corresponds to the coefficients in the Gaussian beam frame[55,56], i.e., the corresponding decomposition of the associated field radiating from the equivalent aperture linked to the current. Numerous techniques exist to calculate the weight function F, either by solving a linear system of equation[56], expressing the function as a projection on the GB frame[55] or using the stationary phase theorem and a steepest descent method[45,47,56,49,52]. Here, we choose the latter but contrary to[57,49,52] we do not calculate it to match the desired RCS but to match the asymptotic ray solution following[45,48]. Here, as in[48], we match the GBS field to our Green kernel of the form

$$u^\infty(M) = \frac{\exp(jkR)}{4\pi R}. \tag{13}$$

Thus, using a saddle point method[45], we can match the GB to the asymptotic solution (13) to obtain

$$F(\phi) = \frac{k\omega\omega_0^2}{2c_0}, \tag{14}$$

which does not depend on ϕ but only on the central take-off angle of the GB ϕ_0[46]. The main idea here is that after applying the conformal mesh, we calculate the associated propagation from each point source (current), which now corresponds up to a constant to our matched GB. Finally since F only depend on ϕ_0 equation (12) is finally approximated by

$$u(M) = 2\pi F(\phi_0) \sum_{k=1}^{N} u_{\phi_k}(s_k, q_{1,k}, q_{2,k}) \phi_k \sin(\phi_k). \tag{15}$$

By using this equivalence, we have a complete numerical, or semi-analytic, expression that does not depend on the underlying mesh and where we do not need to recompute F for each target, making it advantageous compared to[49,52]. In addition this allows to relax the far-field criteria that was necessary for the GBS[49,52] to the size of the mesh cell such that $r \geq 2D_{\text{cell}}^2/\lambda$.

Inserting (15) in (11) finally leads to the following complete formula

$$\mathbf{E}^s = 2\pi jk\mathbf{k}_s \times \sum_{\tau \in S_h} \left(\mathbf{k}_s \times \mathbf{J}(\mathbf{R}'_\tau)\right) F(\phi_0)|\tau| \sum_{p=1}^{N} u_{\phi_p}(s_p, q_{1,p}, q_{2,p}) \phi_p \sin(\phi_p). \tag{16}$$

It shall be noted that since u always exists, contrary to the Green kernel, we have here an expression that is free of singularities. Furthermore, the Gaussian kernel links the current on the target to the observation point, thus this expression directly works in the mono and bi-static cases without any modifications. Indeed, accounting for the source incident angle is performed by expressing the induced current $\mathbf{J}(\mathbf{R}')$ in terms of the incident field $\mathbf{E}^i(\mathbf{R}')$, it acquires a spatially varying phase factor $e^{jk\mathbf{k}_i \cdot \mathbf{R}'}$, depending on the position of the cell center over the target surface S. This is equivalent to a phase steering operation across the scatterer, analogous to the phase shifts applied in array beamforming. Furthermore, the distance s_p shall also be computed from the center of the considered cell $\tau \in S_h$ to the observation point M. The pseudo-code 1 sums up the proposed method. First, for a given distance we compute the optimal beam waist and the weight function. Then, we loop over each facets, either quadrangles or triangles, and compute the current from the incident field. After that we compute the contribution of the gaussian beams at M (observation point) with a quadrature, loop over the beams, and finally we normalize the field. This code naturally handle monostatic and bistatic configuration, since the gaussian beam are launched toward the observation direction with a take-off angle $\phi_p \leq \phi_{\max} = \pi/4$, and the current is calculated from the incident direction contrary to other previous works on the GBS for RCS computations[57,49,52]

Accounting for a dielectric or dielectric-coated target is performed through the Fresnel coefficient, as for the PO[59,60,61,62,63] with

$$\begin{aligned} \mathbf{J} &= (1 + R_H(\theta_i))\mathbf{n} \times \mathbf{H}^i, \\ \mathbf{M} &= -(1 + R_E(\theta_i))\mathbf{n} \times \mathbf{E}^i, \end{aligned} \tag{17}$$

Algorithm 1 Semi-analytic Gaussian beam summation.

```
Require: k_i, k_s                ▷ Desired incident and scattering directions
Require: H^i                     ▷ Incident magnetic field to compute the current
Require: M = (s, θ_s, φ_s), ω, k, S_h, φ_p = [0, π/4], N_GB
  ω_0 = sqrt(2c_0/ω) s
  F(φ_0) = k ω ω_0^2 / (2c_0),
  for τ ∈ S_h do                 ▷ Loop over the mesh
     (x', y') ← centroid of τ
     J(x', y') = 2n × H^i(x', y')   ▷ Compute the current at the patch centroid
     for p ≤ N_GB do             ▷ Loop to compute the Gaussian beams contribution at M
        s_p ← distance from the centroid of τ to M
        φ_p = Φ_p[p]
        u_GB += u_{φ_p}(s_p, q_{1,p}, q_{2,p}) φ_p sin(φ_p)
     end for
     u[i] += (k_s × J(x', y')) F(φ_0) |τ| u_GB
  end for
  u = 2πjk k_s × u               ▷ Final normalization of the field
```

where R_i is the reflection coefficient that depends on the incident angle and the polarization. Indeed, using the discretization provided from the semi-analytic method we derived, we can assume a tangent plane approximation where the Fresnel coefficients can be applied at each surface element. Thus, we can consider the material to be uniform locally. Meshing the surface of the object also allows us to consider different materials over the target, contrary to [52] where only uniform and thick dielectric materials could be considered. Furthermore, the currents can be directly introduced in (16) to account for a dielectric target with

$$\begin{aligned} R_\perp &= \frac{k_{in,z} - k_{tr,z}}{k_{in,z} + k_{tr,z}}, \\ R_\parallel &= \frac{n_1 k_{in,z} - n_2 k_{tr,z}}{n_1 k_{in,z} + n_2 k_{tr,z}}, \end{aligned} \tag{18}$$

where $\perp$ and $\parallel$ correspond to the considered polarization, n_i to the refractive index in the medium i, $k_{in_z} = -k_1 \cos(\theta_i)$, the projection on the normal vector of the incident wave vector, and $k_{tr,z} = \sqrt{k_2^2 - k_1^2 \sin^2(\theta_i)}$, with $k_i = k_0 n_i$, with n_i the index of refraction in the media i. In the case of a dielectric coating, the reflection coefficient is computed [64] as follows, assuming infinite reflections

$$R = \frac{R_{1,2} + R_{2,3} \exp(-2j\beta)}{1 + R_{1,2} R_{2,3} \exp(-2j\beta)}, \tag{19}$$

where $R_{i,j}$ is the reflection coefficient, computed with (18), for the medium i and j, and

$$\beta = 2\pi n_2 d \sqrt{1 - (n_1/n_2)^2 \sin^2(\theta_i)}/\lambda, \tag{20}$$

where d is the thickness of the coating. The latter can be generalized to consider more media for the coating. Furthermore, when a PEC is coated with a dielectric, we have $R_{2,3} = \pm 1$. We can also truncate the series that leads to (19) to account for only a certain number of reflections. Indeed, depending on the coating thickness, accounting for an infinite number of reflections could be unnecessary. Furthermore, we could follow the works of [65,66,67] to account for other coating such as metamaterials or anisotropic medium but the main idea of the paper is to generalized the GBS [52] to account for dielectric coating and for the bistatic case first before handling more complicated structures and materials.

We can also, as for geometrical optics or PO, accounts for diffraction effect through the GTD [68,69] or UTD [70,71]. Using the semi-analytical approach the latter is quite easy. Indeed, we consider a mask of the edges triangular or quadrangular patch and apply the GTD or UTD to these cells. Then, we add this contributions to the overall scattering field leading to a method denoted by GBS+GTD that improve the accuracy near the edges. For more complicated structures, we shall first apply a ray launching in order to obtain the visible patches, then find the ones where diffraction occurs to obtain the associated mask and then calculate the contribution from each facets using the GBS and the UTD when diffraction occurs.

2.4 | Time complexity comparison to other methods

Now let us compare the time complexity of the proposed semi-analytic GBS method to other conventional methods, such as PO and the Method of Moments (MoM).

First, we derive the complexity of the GBS method. For each observation direction θ_s, we need to compute the contributions of all Gaussian beams (N_{GB}) over all facets (N_{tri}), leading to a time complexity of

$$\mathcal{C}_{GB} = \mathcal{O}(N_{\text{obs}} N_{GB} N_{\text{tri}}), \tag{21}$$

where N_{obs} is the number of observation angles. For the PO method, the complexity is linked to the quadrature order N_{quad} used to evaluate the surface integrals:

$$\mathcal{C}_{PO} = \mathcal{O}(N_{\text{obs}} N_{\text{quad}} N_{\text{tri}}). \tag{22}$$

In general, the GBS method is computationally more expensive since $N_{GB} \geq N_{\text{quad}}$. Nonetheless, this additional cost comes with several advantages: GBS naturally regularizes singularities, particularly near shadow boundaries or edges, and allows modeling of finite-width or localized sources beyond plane waves [46].

Finally, both high-frequency methods have a drastically reduced complexity compared to MoM, which requires inverting a dense system of size N_{tri}, leading to a leading-order cost of $\mathcal{O}(N_{\text{tri}}^3)$. Therefore, the semi-analytic GBS method can be seen as an intermediate approach between the fast but approximate PO method and the fully accurate but computationally intensive MoM.

3 | RESULTS

This section is devoted to numerical tests to both validate the method and highlight its advantages. All the numerical experiments have been performed on a standard desktop computer. Furthermore, here the particular case of $\phi = 0°$ has been considered, but all can be generalized.

3.1 | Free-space test

We begin by validating our Gaussian beam in the simplest case, a free-space propagation from a point source. Indeed, this allows us to verify that the weight function F is valid and to compare the result with N_{GB} increasing in terms of both accuracy and computation time. Furthermore, it highlights the fact that Gaussian beams are singularity-free.

The parameters of the scenario are as follows. The frequency is set to 1 GHz. We consider Gaussian beams with $\omega_0 = 5\lambda$ and $N_{GB} \in [10, 50, 100, 200, 400, 800]$ for the number of gaussian beams. In Figure 4, we plot the field computed either with the analytic expression, i.e., the Green kernel, or with the Gaussian beam summation for different positions of M, i.e., radius $r \in [-100, 100]$ m. We also plot the computation time needed for the different number of gaussian beams in Figure 5.

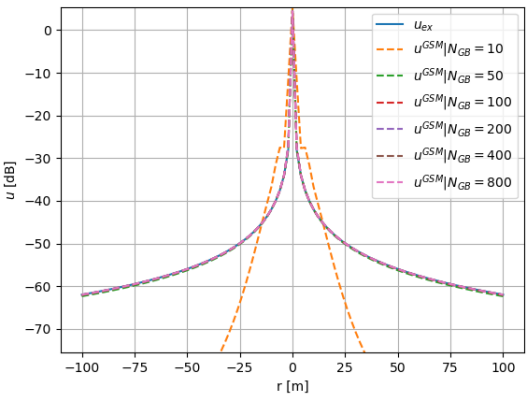

FIGURE 4 Ray asymptotic solution and GBS method comparison in free-space for different receiving position r.

The first conclusion is that the GB expansion closely matches the asymptotic solution for r increasing, as expected from the calculation of F with $N_{GB} \geq 50$. Secondly, we can see that with the GBS, no singularity occurs near $r = 0$, whereas the ray asymptotic solution, based on the Green kernel, cannot be computed for this point. Finally, as expected the computation time is increasing linearly with the number of gaussian beams in the expansion. Thus, the GBS expansion is validated in this case. For a more thorough study on the convergence with the number of Gaussian beams we refer the interested readers to[45,72,52], and from now on we use $N_{GB} = 200$ since it gives good accuracy while keeping the computation time low.

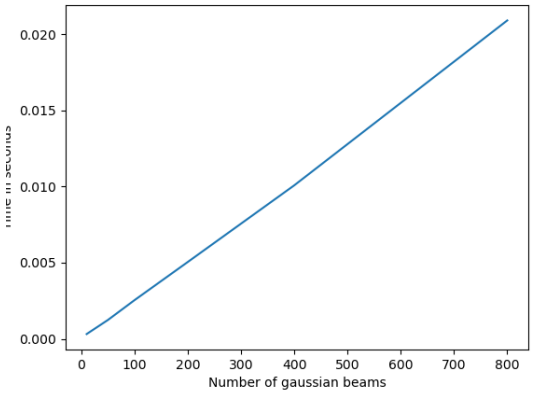

FIGURE 5 Computation time of the GBS method with the number of gaussian beams.

3.2 | RCS of a flat plate in the monostatic case

Here, we study the case of a flat plate, either a PEC, a dielectric, or one with a dielectric coating. We aim to validate the semi-analytic GBS method in this case. To do so, we compare our results to the analytic result in a PO setting, which is widely used in this case. Furthermore, in this case, we use the optimal value for ω_0 [46,47,52].

Firstly, we validate our proposed approach on a PEC by performing a convergence analysis over the mesh size, i.e., the number of facets. To do so we consider a frequency of 10 GHz and a flat plate of size $a = 5\lambda$ and $b = 3\lambda$. We compare our results to a direct PO RCS calculation, i.e., without discretization, i.e. the analytic formula in a PO setting. In particular, for the proposed GBS we consider a uniform quadrangular mesh, with $N = N_x = N_y$, and increase the number of elements over each axis from $N = 10$, i.e. $h_x = \lambda/2$, to $N = 50$, i.e. $h_x = \lambda/10$, while keeping all the gaussian beam parameters the same. The results are also compared in terms of both accuracy and computation time to the usual PO with a midpoint quadrature, as for the GB expansion.

In Figure 6, we plot the normalized RCS, by the area of the target, for the analytic PO in plain line and for the proposed semi-analytic GBS method in dotted lines for different numbers of facets, while the numerical PO is plotted in dotted line. We also plot in Figure 7 the evolution of the l^2-error with the mesh grid for both the GBS and the numerical PO methods by comparison with the analytic PO. Finally, in Figure 8 we plot the computation needed for each method for the number of discretization points over each axis.

The first conclusion is that the method works well. Indeed, Figure 7 shows that the l^2 error is low and decreases with the number of facets, as expected. It is emphasized with Figure 6 where we can see that with N increasing, the computed RCS with the GBS method tends toward the true RCS calculated with the analytic PO. The higher difference for $N = 10$ is normal since over the x-axis we have a mesh size of $\lambda/2$. While for $N = 50$, the two curves are almost perfectly matching. Furthermore, the maximum is at -22 dB as expected from a direct calculation using

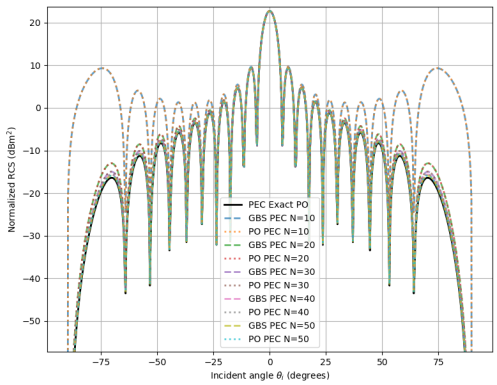

FIGURE 6 Normalized RCS for a PEC flat plate computed with the analytic PO, numerical PO or with the proposed GBS method for different mesh sizes in a monostatic configuration.

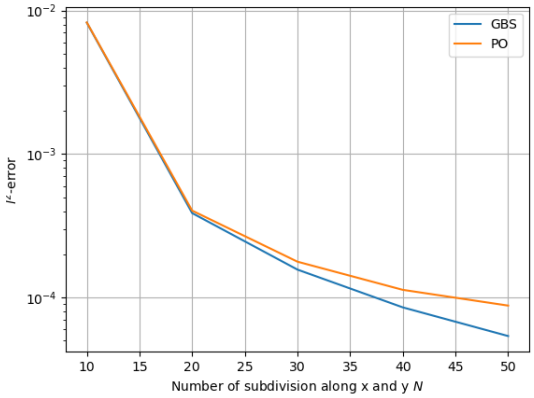

FIGURE 7 Evolution of the l^2-error of the proposed approach and the numerical PO, with analytic PO as reference, with the number of cells N along both directions.

the canonical formula for a PEC rectangular plate. This result is also in line with the ones obtained through experiments in[49,50,52]. In addition, we can see that the error is decreasing faster with the GBS method compared to the computational PO. Nonetheless, this comes at the cost of computation time as can be seen in Figure 8. Nonetheless, from the previous test, the GBS computation time could be reduced by half by considering half the number of GB while keeping a good accuracy. From now on we only keep the analytic PO as reference, that will thus be called PO so that the figure are clear. Indeed, the conclusion in terms of computation time and accuracy remain the same for the following tests.

Secondly, we validate the method for dielectric material at $f = 1$ GHz. In this case, we study different dielectric materials with the following parameters: a dry ground $\varepsilon_r = 20$ and $\sigma = 0.02$ S/m; the sea with $\varepsilon_r = 80$ and $\sigma = 5$, and FR4, which is a widely used material with $\varepsilon = 4.4$ and $\tan\delta = 0.03$. For the first two, we consider an infinite substrate so that we use the Fresnel coefficient, for the FR4 we consider both an infinite substrate but also FR4 as a coating. A flat plate of size

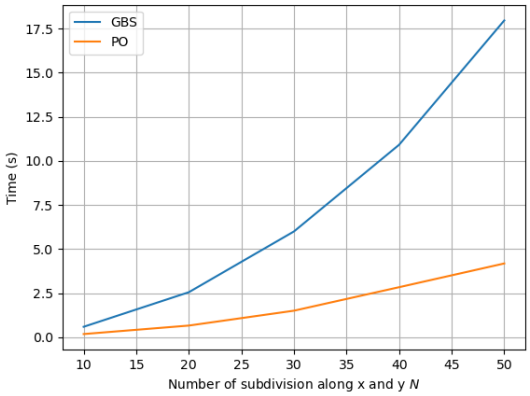

FIGURE 8 Evolution of the computation time of the proposed approach and the numerical PO, with the number of cells N along both directions.

$a = 8\lambda$ and $b = 5\lambda$ is considered in all cases, and the discretization is performed with $N_x = N_y = 70$. For the coating, we set the thickness to $h = 0.1\lambda$. We plot in Figure 9 the results for the different cases, for each material, the plain line corresponds to the PO while a dotted line corresponds to the proposed GBS approach. We also show the result for a PEC for comparison.

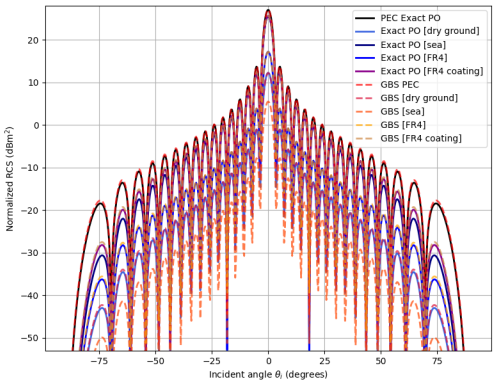

FIGURE 9 Normalized RCS for a flat plate with different materials considered computed with the PO or with the proposed GBS method in a monostatic configuration.

We can see that the proposed method works well in this case. Indeed, the results obtained with the semi-analytic GBS closely match the PO calculations even for dielectric or dielectric-coated materials. In addition, for all the considered cases, the results are in line with physical expectations, as the dielectric coating allows for a reduction in the RCS. However, with $h \ll \lambda$, we are still close to a PEC. Additionally, we can note that the difference increases with the incident angle, as expected. For all the other materials, the differences in terms of normalized RCS are directly explained by their respective difference in permittivity.

In conclusion, the proposed semi-analytic GBS formulation has been validated in the mono-static case.

3.3 | RCS of a flat plate in the bistatic case

In this case, we perform the same analysis as before, except that we consider a triangular mesh, using the Delaunay triangulation, of the plate.

First, we consider a PEC plate of size $a = 5\lambda$ and $b = 3\lambda$ at $f = 1$ GHz. The illuminating plane wave comes from an angle of $\theta_i = 30°$. The triangulation is performed for an increasing number of facets to assess the convergence of the method. As before, in Figure 10 we plot the RCS computed with the PO or with the proposed approach for different N, while in Figure 11 we show the convergence of the method with N, i.e., the mesh size.

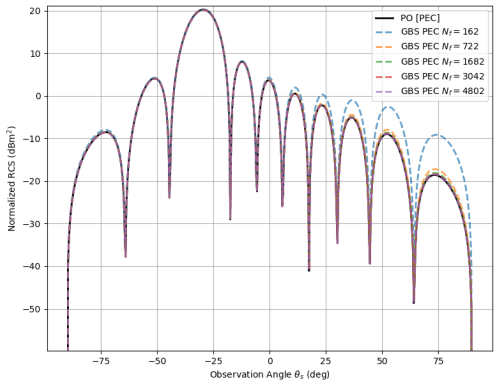

FIGURE 10 Normalized RCS for a PEC flat plate computed with the PO or with the proposed GBS method for different numbers of triangular facets in a bistatic case.

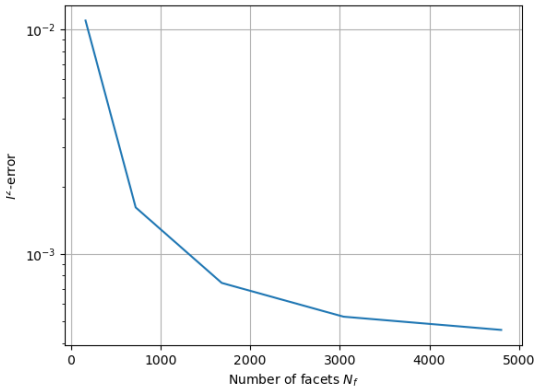

FIGURE 11 Evolution of the l^2-error of the proposed approach, with PO as reference, with the number of facets N_f.

As for the monostatic case, we can see that the method works well in the bistatic case. Indeed, the l^2-error converges with the number of facets, while we can see that the RCS computed with the GBS tends to match the RCS calculated with the PO as N_f increases. Finally, as expected, the maximum of the RCS is at $\theta_s = -\theta_i$.

Now, as before, we consider the case of different materials: a dry ground, the sea, an FR4 plate, and an FR4-coated PEC. The idea is to validate our approach in the case of considering dielectric objects. As in the previous test, the first three are considered infinite while the last is a finite substrate over a PEC. The frequency is set at $f = 10$ GHz. In addition, the incident angle for the incoming wave is $\theta_i = -40°$. The dielectric parameters remain the same as before. The size of the plate is $a = 10\lambda$ and $b = 7\lambda$ while the thickness is set to $h = 0.25\lambda$ in case of the FR4 coating. The number of facets is set to $N_f = 4802$ to ensure convergence. The results are plotted in Figure 12 with the same legend as for Figure 9.

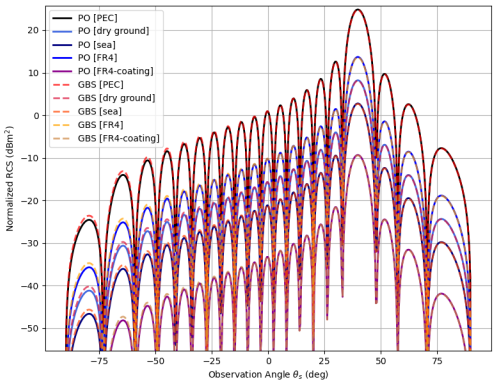

FIGURE 12 Normalized RCS for a flat plate with different materials considered computed with the PO or with the proposed GBS method in a bistatic configuration.

Here, we can see that the method works well. Indeed, the results obtained with the semi-analytic GBS approach closely match the ones directly calculated with PO. We obtain, as expected, a maximum of RCS at $\theta_s = 40° = -\theta_i$. Furthermore, for all materials, the reduction in RCS is in line with the monostatic cases. In this case, for the FR4 coating, the reduction in RCS is increased, which is normal since we use a thickness of $\lambda/4$, which is an extinction distance. Therefore, the method is also validated in this case.

3.4 | Accounting for diffraction through the GTD

As a final numerical experiments, we show in a bistatic case that we can account for diffraction on the edges of our plat through the GTD [73,68]. In particular here we use the one derived by Keller [73], and use the method prescribed at the end of Section 2.3. Note that here this is a

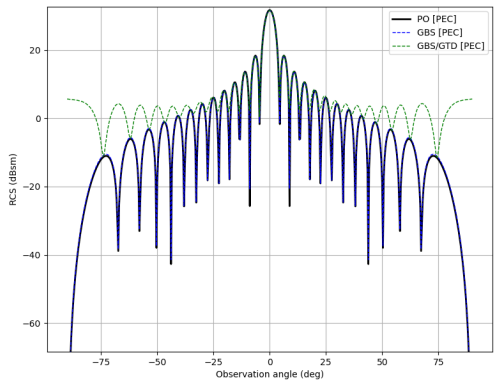

FIGURE 13 Normalized RCS for a flat PEC plate calculated with the PO (analytical), the GBS and the GBS+GTD methods.

simple test case to show that is achievable, and that the generalization to complicated structures is possible.

For this, we consider a flat PEC plate of size $a = 13\lambda$ and $b = 9\lambda$ in a bistatic configuration with an incident wave coming from $\theta_i = 0°$ and a frequency of $f = 10$ GHz. In Figure 13, we compare the PO (as before the analytic formula for the plate), with the GBS and the GBS+GTD methods. For the mesh we consider 4802 triangles. The GTD is only applied to the one that are one the boundary. We expect the GTD to correct the scattered field near the edges so that we do not decrease rapidly to 0. For the

As expected, using the GTD allows to consider the effect of diffraction near the edge and to keep accurate results in the specular direction. Furthermore, this results are in line with experimentation that have been performed in [72] since we retrieve a similar difference between the maximum and the diffraction lobes. Nonetheless, this could be improved using the UTD [70] or the Michaeli's method of equivalent current [74].

3.5 | Accounting for uncertainty in the dielectric parameters of the target

To conclude the numerical experiments, we use the proposed GBS approach to perform uncertainty quantification over the material dielectric parameters. A direct way to do that would be to use the Monte-Carlo method. Indeed, with the latter we compute N_s samples of the output from N_s samples of the inputs using any method as a black-box, i.e., a non-intrusive method. In addition, the law of large number ensure the convergence of the method. Nonetheless, it usually requires a very large number of samples to converge, even if accelerated, using quasi-Monte-Carlo methods [75]. Here, we propose to use the polynomial chaos expansion (PCE) to expedite the results [76,77]. Indeed, Ghanem *et al.* [76] proposed an intrusive stochastic finite element strategy that allows to handle uncertainty in the code but necessitate to introduce a new code. On the other hand, Sudret [77] proposed a way to use the PCE with non-intrusive methods, either using regression or projection, that allow to keep the code intact. Thus here, we keep the proposed semi-analytic GBS method as a black-box, as with Monte-Carlo, and use a non-intrusive projection-based PCE method [77], that we adapt to our problem.

Here, we assume that the material dielectric parameter and thickness are not perfectly known, i.e., that $\Re(\varepsilon)$, the real part of ε, and $\Im(\varepsilon)$, its imaginary part, are random values and that d is also a random variable. From a physical point of view, we can assume that they all need to be positive, since we do not consider plasma or metamaterials here, and d is a thickness. Nonetheless, all is easily generalizable to other cases or inputs. In this case, we can assume that the three are following log-Normal distribution, since they need to be positive, and thus we can decompose them using probabilistic multivariate Hermite polynomials as

$$\begin{aligned}\Re(\varepsilon) &= \sum_i \alpha_i^{\mathrm{re}} \psi_i(\zeta),\\ \Im(\varepsilon) &= \sum_i \alpha_i^{\mathrm{im}} \psi_i(\zeta)\\ d(\varepsilon) &= \sum_i \alpha_i^{\mathrm{d}} \psi_i(\zeta),\end{aligned} \tag{23}$$

where ψ_i are Hermite polynomials of a reduced centered normal law ζ, and α_i the associated coefficients.It shall be noted that in the case of other distribution the expansion is the same, and we only change the basis using the Wiener-Askey scheme [78]. For example, we use Legendre polynomial for uniform law and keep the Hermite ones for normally distributed variables. In case of stochastic variables, i.e. that depend also on the position, we first apply a Kosambi-Karhunen-Loève [79] expansion and then the PCE. For ε this can then be simplified to

$$\varepsilon = \sum_i (\alpha_i^{\mathrm{re}} - j\alpha_i^{\mathrm{im}})\psi_i(\zeta), \tag{24}$$

where the α_i are known [77]. The electromagnetic field is decomposed in the same basis, leading to

$$E^s = \sum_i E_i^s(r)\psi_i(\zeta), \tag{25}$$

where the coefficients are unknown. Nonetheless, using the orthogonality of the PCE decomposition, we have

$$E_i^s(r) = \frac{\mathbb{E}(E^s\psi_i(\zeta))}{\mathbb{E}(\psi_i(\zeta)^i)}, \tag{26}$$

where $\mathbb{E}$ is the expectation. In this equation, only the numerator is not known, but it can be easily computed numerically using a Gauss-Hermite quadrature of order d. Then, the usual moments can be computed from the coefficients, i.e., $E_0^s = \mathbb{E}(E^s)$, or the surrogate model (25) can also be used to compute samples rapidly and thus any statistical information such as confidence intervals or Sobol's indices. Note that for the RCS we need to compute $\mathbb{E}(|E^s|)$, since contrary to [77] we manipulate complex valued functions, so that we can have the mean or the standard deviation. To do this, we also use a Gauss quadrature.

For the test, we consider the FR4 material as uncertain. For the permittivity, its real and imaginary part now follow log-Normal distribution, since they are positive, with a mean determined from the deterministic

parameters, i.e., they are $\varepsilon = 4.4$ and $\tan\delta = 0.03$, and their standard deviation set to a variation coefficient $c = \mu/\sigma = 30\%$ and 20% respectively. For the thickness we consider a mean of 0.02λ and a variation of 5%. The rest of the parameters remain the same as for the previous case. In Figure 14 (a), we plot the RCS computed when no uncertainty is accounted for, the mean computed through the PCE decomposition, and the one calculated using the Monte-Carlo method with 200000 samples. In (b), a zoom is performed around the maximum. In addition, the 90% confidence interval is plotted as a blue area around the mean for the PCE case.

First of all, in terms of computation time, the PCE proposed approach is $30\times$ more rapid than the Monte-Carlo based one. Furthermore, as can be seen in Figure 14, the RCS computed with both methods are matching, which is also confirmed from the $l2$−error on the 1st and 2nd statistical moments that are 3.2×10^{-6} and 5.7×10^{-7}, respectively. In addition, from the zoom, we can see that this approach is necessary since the results when considering the FR4 dielectric parameters as deterministic are not in line with the PCE or MC ones, even if the variation are not so high. In addition, this method also allows to compute other important statistical information such as the 90% confidence interval plotted as a blue area around the mean here. Indeed, this information is important when optimizing target RCS for example and to be able to know if we respect the specification. Thus, this method paves the way to rapidly perform uncertainty quantification for RCS prediction with the GBS.

4 | DISCUSSION AND CONCLUSIONS

In this work, we have proposed a semi-analytic Gaussian beam summation (GBS) method to compute the radar cross section (RCS) of objects in both monostatic and bistatic configurations. We have also demonstrated how to efficiently incorporate uncertainty in the dielectric parameters of the target. In addition, we proposed a way to introduce diffraction, with a numerical example, to be able to account for more complicated structures in the future.

The approach relies on replacing plane waves, as in physical optics (PO), with Gaussian beams to remove the singularity of the Green's kernel. By representing the field as a superposition of Gaussian beams, we obtain a singularity-free formulation that can be solved numerically using quadrature, with the complex weight function evaluated via a saddle-point method. Importantly, we showed that the method naturally extends to the bistatic case, which—to the best of our knowledge has not previously been investigated in the context of GBS.

Numerical experiments in the S- and X-bands have confirmed the validity of the method across a range of configurations. Indeed, the results show both numerical convergence and a low error compared to PO, even in the presence of dielectric materials or dielectric-coated targets. Furthermore, we introduced a non-intrusive polynomial chaos expansion (PCE) approach to quantify uncertainty in the dielectric properties, which yielded highly accurate results and a drastic reduction of time compared to the Monte-Carlo method.

Nonetheless, the method has some limits. Removing the singularity comes at the cost of an increased time complexity, even if this could be reduced in the future by optimizing the number of gaussian beams used. In addition, we only treated simple structures since we wanted to validate the method, but there is still some work to do to be able to treat realistic target. Indeed, we will first need to accelerate the code by parallelizing it, as for PO, and using octree or quadtree methods [80] for example. Also, the GBS can in theory be used for any input sources, we could improve the matching of the weighting functions for this case, or also to directly accomodate for the diffraction by matching the diffracted rays. Another limit of the current method is that only locally homogeneous material can be accounted for, but this can be improved by adapting the Fresnel reflection coefficient to the case studied.

This study, therefore, opens the way for applying GBS to bistatic scenarios while accounting for dielectric materials. Nonetheless, several directions remain for future work. Diffraction phenomena have only been introduced using the GTD and we are currently developing their treatment for relevant facets using more appropriate diffraction theory [74]. In parallel, experimental validation with measured data is ongoing. We are also investigating uncertainty quantification for additional parameters, such as target geometry, which is of interest in the case of stealth targets. Finally, we are considering extensions to more realistic scenarios by hybridizing the method with Gaussian beam solvers for the parabolic wave equation [81]. In conclusion the proposed method can be seen as an in between the PO and the MoM for RCS computation.

AUTHOR CONTRIBUTIONS

Thomas Bonnafont: Conceptualization (lead), Formal analysis (lead), Investigation, Formal Analysis (lead), Methodology (lead), Software (lead), Validation, Writing - Original Draft Preparation. Mira Kaissar Abboud: Conceptualization, Methodology. Ali Khenchaf: Conceptualization, Validation, Funding Acquisition (lead), Project Management (lead), Writing - Review & Editing. Philippe Pouliguen: Validation, Writing - Review & Editing.

ACKNOWLEDGMENTS

The authors would like to thank the AID-DGA (Defense Innovation Agency - Directorate General of Armaments) for their support of this research work carried out within the framework of the HyMEF project

FINANCIAL DISCLOSURE

None reported.

CONFLICT OF INTEREST

The authors declare no potential conflict of interests.

REFERENCES

1. Blyakhman AB, Runova IA. Forward scattering radiolocation bistatic RCS and target detection. In: IEEE. 1999:203–208.
2. Hwang JT, Hong SY, Song JH, Kwon HW. Radar cross section analysis using physical optics and its applications to marine targets. *Journal of Applied Mathematics and Physics*. 2015;3(2):166–171.

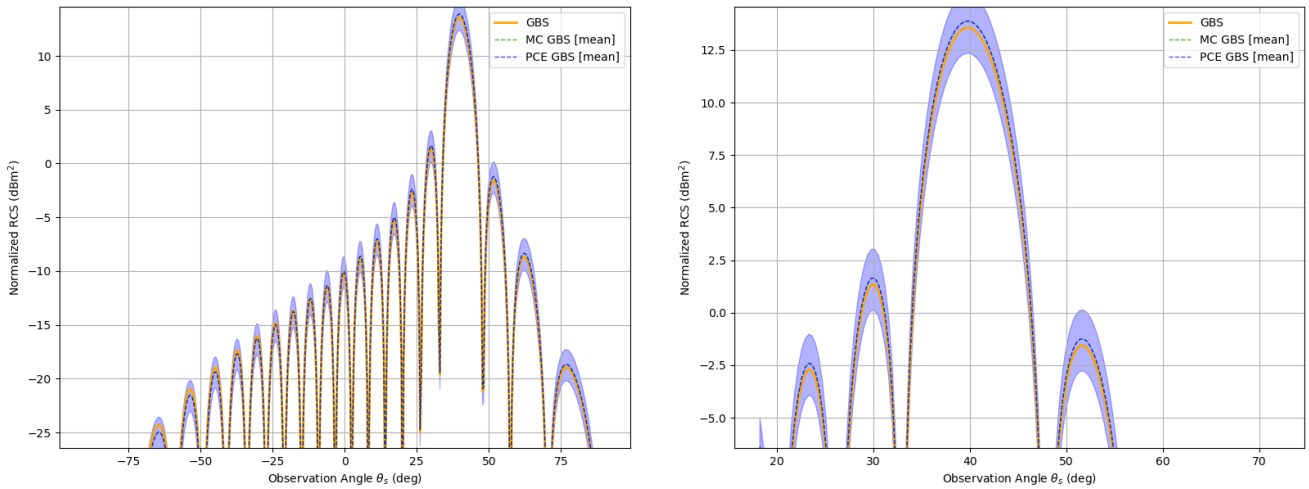

(a) Normalized RCS over the whole angle range.

(b) Zoom at the maximum of the normalized RCS.

FIGURE 14 Normalized RCS for a flat plate of FR4 whose parameters are considered uncertain in a bistatic configuration.

3. Ghanmi H, Khenchaf A, Comblet F. Bistatic scattering from a contaminated sea surface observed in C, X, and Ku bands. In: . 9240. SPIE. 2014:48–56.
4. Zheng H, Gou C, Khenchaf A, Wang Y, Zhang Y. Retrieving Oil-Water Mixture Ratios of Marine Oil Spills From L-Band SAR Imagery. *IEEE Transactions on Geoscience and Remote Sensing*. 2022;60:1–11.
5. Bonnafont T, Khenchaf A. Long-range electromagnetic propagation above a polluted sea surface: hybrid modeling. *IEEE Geoscience and Remote Sensing Letters*. 2024.
6. Chiang CY, Chen KS. Simulation of complex target RCS with application to SAR image recognition. In: IEEE. 2011:1–4.
7. Cakoni F, Colton DL. *A qualitative approach to inverse scattering theory*. 767. Springer, 2014.
8. Pinto J, Matthews J, Sarno G. Stealth technology for wind turbines. *IET radar, sonar & navigation*. 2010;4(1):126–133.
9. Hamel P, Adam JP, Kubické G, Pouliguen P. Design of a stealth wind turbine. In: IEEE. 2012:1–4.
10. Jang HK, Choi WH, Kim CG, Kim JB, Lim DW. Manufacture and characterization of stealth wind turbine blade with periodic pattern surface for reducing radar interference. *Composites Part B: Engineering*. 2014;56:178–183.
11. Li M, Bai J, Li L, Meng X, Liu Q, Chen B. A gradient-based aero-stealth optimization design method for flying wing aircraft. *Aerospace Science and Technology*. 2019;92:156–169.
12. Li M, Chen J, Feng X, Qu F, Bai J. An efficient adjoint method for the aero-stealth shape optimization design. *Aerospace Science and Technology*. 2021;118:107017.
13. Zikidis K, Skondras A, Tokas C. Low observable principles, stealth aircraft and anti-stealth technologies. *Journal of Computations & Modelling*. 2014;4(1):129–165.
14. Kim SH, Lee SY, Zhang Y, Park SJ, Gu J. Carbon-based radar absorbing materials toward stealth technologies. *Advanced Science*. 2023;10(32):2303104.
15. Usai P, Borgese M, Costa F, Monorchio A. Hybrid physical optics-MoM-ray tracing method for the RCS calculation of electrically large objects covered with radar absorbing materials. In: IEEE. 2018:145–146.
16. Harrington RF. *Field computation by moment methods*. Wiley-IEEE Press, 1993.
17. Yan Y, Zhang Y, Liang CH, Zhao H, Garcia-Donoro D. RCS Computation by Parallel MoM Using Higher-Order Basis Functions. *International Journal of Antennas and Propagation*. 2012;2012(1):745893.
18. Gibson WC. *The method of moments in electromagnetics*. Chapman and Hall/CRC, 2021.
19. Yee KS, Chen JS. The finite-difference time-domain (FDTD) and the finite-volume time-domain (FVTD) methods in solving Maxwell's equations. *IEEE Transactions on Antennas and Propagation*. 2002;45(3):354–363.
20. Chaudhury B, Chaturvedi S. Three-dimensional computation of reduction in radar cross section using plasma shielding. *IEEE Transactions on Plasma Science*. 2005;33(6):2027–2034.
21. Sullivan DM. *Electromagnetic simulation using the FDTD method*. John Wiley & Sons, 2013.
22. Cakir G, Cakir M, Sevgi L. An FDTD-based parallel virtual tool for RCS calculations of complex targets. *IEEE Antennas and Propagation Magazine*. 2014;56(5):74–90.
23. Gaucher S, Guiffaut C, Bui N, Reineix A, Cessenat O. Angle-dependent face-centered SIBC model of metamaterial in conformal FDTD methods. *IEEE Transactions on Antennas and Propagation*. 2023;71(9):7438–7446.
24. Petitjean B, Lohner R, Devore C. Finite element solvers for Radar Cross-Section (RCS) calculations. In: AIAA. 1992:455.
25. Venkatarayalu NV, Gan YB, Zhao K, Lee JF. Fast monostatic RCS computation in FEM based solvers using QR decomposition. In: IEEE. 2006:1–5.
26. Jin JM. *The finite element method in electromagnetics*. John Wiley & Sons, 2015.
27. Soudais P. Computation of the electromagnetic scattering from complex 3D objects by a hybrid FEM/BEM method. *Journal of Electromagnetic Waves and applications*. 1995;9(7-8):871–886.
28. Dodig H. A boundary integral method for numerical computation of radar cross section of 3D targets using hybrid BEM/FEM with edge elements. *Journal of Computational Physics*. 2017;348:790–802.
29. Lee SW. Electromagnetic reflection from a conducting surface: Geometrical optics solution. *IEEE Transactions on Antennas and Propagation*. 1975;23(2):184–191.
30. Mittra R. Numerical and asymptotic techniques in electromagnetics. *New York*. 1975;3.

31. Deschamps GA. Ray techniques in electromagnetics. *Proceedings of the IEEE*. 2005;60(9):1022–1035.
32. Bouche D, Molinet F, Mittra R. *Asymptotic methods in electromagnetics*. Springer Science & Business Media, 2012.
33. Asvestas JS. The physical optics method in electromagnetic scattering. *Journal of Mathematical Physics*. 1980;21(2):290–299.
34. Knott EF, Shaeffer J, Tuley MT. Radar cross section. In: , , Artech House Norwood, 1988:444–448.
35. De Adana FS, Diego IG, Blanco OG, Lozano P, Catedra MF. Method based on physical optics for the computation of the radar cross section including diffraction and double effects of metallic and absorbing bodies modeled with parametric surfaces. *IEEE Transactions on Antennas and Propagation*. 2004;52(12):3295–3303.
36. Chen S, Yue K, Hu B, Guo R. Numerical simulation on the radar cross section of variable-sweep wing aircraft. *Journal of Aerospace Technology and Management*. 2015;7(2):170–178.
37. Hamel P, Adam JP, Béniguel Y, Kubické G, Pouliguen P. Radar cross section evaluation of a wind turbine, based on an asymptotic method. In: IEEE. 2016:1–3.
38. Ufimtsev PY. Elementary edge waves and the physical theory of diffraction. *Electromagnetics*. 1991;11(2):125–160.
39. Griesser T, Balanis C. Backscatter analysis of dihedral corner reflectors using physical optics and the physical theory of diffraction. *IEEE Transactions on Antennas and Propagation*. 2003;35(10):1137–1147.
40. Ufimtsev PY. *Fundamentals of the physical theory of diffraction*. John Wiley & Sons, 2014.
41. Michaeli A. Equivalent edge currents for arbitrary aspects of observation. *IEEE Transactions on Antennas and Propagation*. 1984;32(3):252–258.
42. Michaeli A. Elimination of infinities in equivalent edge currents, Part I: Fringe current components. *IEEE Transactions on Antennas and Propagation*. 1986;34(7):912–918.
43. Michaeli A. Elimination of infinities in equivalent edge currents, Part II: Physical optics components. *IEEE Transactions on Antennas and Propagation*. 1986;34(8):1034–1037.
44. Gordon WB. High frequency approximations to the physical optics scattering integral. *IEEE transactions on antennas and propagation*. 1994;42(3):427–432.
45. Popov MM. A new method of computation of wave fields using Gaussian beams. *Wave motion*. 1982;4(1):85–97.
46. Červenỳ V, Popov MM, Pšenčík I. Computation of wave fields in inhomogeneous media—Gaussian beam approach. *Geophysical Journal International*. 1982;70(1):109–128.
47. Červeny V, others . Gaussian beam synthetic seismograms. *Journal of Geophysics*. 1985;58(1):44–72.
48. Norris A. Complex point-source representation of real point sources and the Gaussian beam summation method. *JOSA A*. 1986;3(12):2005–2010.
49. Leye PO, Khenchaf A, Pouliguen P. The Gaussian beam summation and the Gaussian launching methods in scattering problem. *Journal of Electromagnetic Analysis and Applications*. 2016;8(10):219–225.
50. Ghanmi H, Khenchaf A, Pouliguen P, Leye PO. Experimental results and numerical simulation of the target RCS using Gaussian beam summation method. *Advances in Science, Technology and Engineering Systems Journal*. 2018;3(3):01–06.
51. Ang YX, Lui HS. Scaled-Model Radar Cross-Section Measurement: The Influence of the Scattered Field under Gaussian Beam Illumination—A Theoretical Analysis. *Sensors*. 2023;23(16):7202.
52. Kaissar Abboud M, Khenchaf A, Pouliguen P, Bonnafont T. Computing the Radar Cross-Section of Dielectric Targets Using the Gaussian Beam Summation Method. *Remote Sensing*. 2023;15(14):3663.
53. Mrnka M, Appleby R, Saenz E. Accurate S-parameter modeling and material characterization in quasi-optical systems. *IEEE Transactions on Terahertz Science and Technology*. 2022;12(2):199–210.
54. Chou HT, Pathak PH, Burkholder RJ. Novel Gaussian beam method for the rapid analysis of large reflector antennas. *IEEE Transactions on Antennas and Propagation*. 2001;49(6):880–893.
55. Lugara D, Letrou C, Shlivinski A, Heyman E, Boag A. Frame-based Gaussian beam summation method: theory and applications. *Radio Science*. 2003;38(2):27–1.
56. Chabory A, Sokoloff J, Bolioli S. Physics-based expansion on 3D conformal Gaussian beams for the scattering from a curved interface. *Progress In Electromagnetics Research B*. 2013;54:245–264.
57. Leye P, Khenchaf A, Pouliguen P. Application of Gaussian beam summation method in high-frequency RCS of complex radar targets. In: IEEE. 2016:1–5.
58. Hill NR. Gaussian beam migration. *Geophysics*. 1990;55(11):1416–1428.
59. Baldauf J, Lee S, Ling H, Chou R. On physical optics for calculating scattering from coated bodies. *Journal of electromagnetic waves and applications*. 1989;3(8):725–746.
60. Anastassiu HT. A closed form, physical optics expression for the radar cross section of a perfectly conducting flat plate over a dielectric half-space. *Radio Science*. 2003;38(2):10–1.
61. Nguyen A, Shirai H. Electromagnetic wave scattering from dielectric bodies with equivalent current method. In: IEEE. 2013:744–747.
62. Mohammadzadeh H, Zeidaabadi-Nezhad A, Hossein Firouzeh Z. Modified Physical Optics approximation for RCS calculation of electrically large objects with coated dielectric. *Journal of Electrical and Computer Engineering Innovations (JECEI)*. 2015;3(2):115–122.
63. Polat B, Daşbaşı R. Physical optics scattering by a PEC plate located vertically over a dielectric half-space. *Progress In Electromagnetics Research B*. 2020;88:151–173.
64. Kind R, others . Computation of reflection coefficients for layered media. *Journal of Geophysics*. 1976;42(1):191–200.
65. He JJ, He SY, Zhu GQ, Zhu LK. Physical optics framework for electromagnetic scattering from electrically large targets coated with a uniaxial electric anisotropic medium based on point-source excitation. *Optics Express*. 2021;29(21):33642–33664.
66. Eskandari MR, Eskandari AR. Physical optics approximation of electromagnetic field scattered from large PEC objects covered with chiral metamaterials. *AEU-International Journal of Electronics and Communications*. 2022;147:154142.
67. Rao Z, Zhu G, He S, Li C, Yang Z, Liu J. Simulation and analysis of electromagnetic scattering from anisotropic plasma-coated electrically large and complex targets. *Remote Sensing*. 2022;14(3):764.
68. Pathak PH. *Techniques for high-frequency problems*. Springer, 1988.
69. Bouche DP, Molinet FA, Mittra R. Asymptotic and hybrid techniques for electromagnetic scattering. *Proceedings of the IEEE*. 2002;81(12):1658–1684.
70. Pathak P, Wang N, Burnside W, Kouyoumjian R. A uniform GTD solution for the radiation from sources on a convex surface. *IEEE Transactions on Antennas and Propagation*. 1981;29(4):609–622.
71. Chou HT, Pathak PH, Hsu M. Extended uniform geometrical theory of diffraction solution for the radiation by antennas located close to an arbitrary, smooth, perfectly conducting, convex surface. *Radio Science*. 1997;32(4):1297–1317.
72. Abboud MK, Khenchaf A, Pouliguen P. Gaussian beams formalism for high frequency scattering problems by metallic targets. In: IEEE. 2021:109–112.
73. Keller JB. Geometrical Theory of Diffraction∗. *J. Opt. Soc. Am.*. 1962;52(2):116–130. doi: 10.1364/JOSA.52.000116

74. Michaeli A. Equivalent edge currents for arbitrary aspects of observation. *IEEE Transactions on Antennas and Propagation*. 2003;32(3):252–258.
75. Soboĺ I. Quasi-monte carlo methods. *Progress in Nuclear Energy*. 1990;24(1-3):55–61.
76. Ghanem R, Spanos PD. *Polynomial chaos in stochastic finite elements*, 1990.
77. Sudret B. Polynomial chaos expansions and stochastic finite element methods. *Risk and reliability in geotechnical engineering*. 2014:265–300.
78. Xiu D, Karniadakis GE. The Wiener–Askey polynomial chaos for stochastic differential equations. *SIAM journal on scientific computing*. 2002;24(2):619–644.
79. Wang L. *Karhunen-Loeve expansions and their applications*. London School of Economics and Political Science (United Kingdom), 2008.
80. Deng JY, Guo LX. An Efficient Octree-Based MoM-PO Method for Analysis of Antennas on Large Platform. *IEEE Antennas and Wireless Propagation Letters*. 2015;14:819-822. doi: 10.1109/LAWP.2015.2399372
81. L'Hour CA, Fabbro V, Chabory A, Sokoloff J. 2-D propagation modeling in inhomogeneous refractive atmosphere based on Gaussian beams Part I: Propagation modeling. *IEEE Transactions on Antennas and Propagation*. 2019;67(8):5477–5486.

SUPPORTING INFORMATION

Additional supporting information may be found in the online version of the article at the publisher's website.

DATA AVAILABILITY

Data sharing not applicable to this article as no datasets were generated or analysed during the current study

AUTHOR BIOGRAPHY

empty.pdf

Author Name. Please check with the journal's author guidelines whether author biographies are required. They are usually only included for review-type articles, and typically require photos and brief biographies for each author.